Unraveling Water Solvation Effects with Quantum Mechanics/Molecular Mechanics Semiclassical Vibrational Spectroscopy: The case of Thymidine

Davide Moscato,[†,‡] Giacomo Mandelli,[†,‡] Mattia Bondanza,[¶] Filippo Lipparini,[*,¶] Riccardo Conte,[†] Benedetta Mennucci,[¶] and Michele Ceotto[*,†]

[†]*Dipartimento di Chimica, Università degli Studi di Milano, Via Golgi, 19 - 20133 Milano - Italy*

[‡]*These authors contributed equally*

[¶]*Dipartimento di Chimica e Chimica Industriale, Università di Pisa, Via Giuseppe Moruzzi, 13 - 56124 Pisa - Italy*

E-mail: filippo.lipparini@unipi.it; michele.ceotto@unimi.it

Abstract

We introduce a QM/MM semiclassical method for studying the solvation process of molecules in water at the nuclear quantum mechanical level and with atomistic detail. We employ it in vibrational spectroscopy calculations because this is a tool which is very sensitive to the molecular environment. Specifically, we look at the vibrational spectroscopy of thymidine in liquid water. We find that the C=O frequency red shift and the C=C frequency blue shift, experienced by thymidyne upon solvation, are mainly due to the reciprocal polarization effects that the molecule and the water solvent exert on each other and the nuclear zero-point energy effects. In general, this work

provides an accurate and practical tool to study quantum vibrational spectroscopy in solution and condensed phase, incorporating high-level and computationally affordable descriptions of both the electronic and nuclear problems.

Introduction

All biological processes take place in water and, for this reason, water is considered the "universal solvent". Primarily *in vivo,* solvation in water is pivotal for processes like protein folding, DNA recombination, and to drive fundamental metabolic reactions.[1–4] Therefore, the understanding of the structural and dynamical properties of molecular systems solvated by water is one topic which has implications not only on all branches of chemistry, but also on biology, physics, and materials science. Providing an atomistic and fully quantum mechanical understanding of these phenomena is crucial and very valuable.

Several different approaches have been employed in the past to study water solvation. Many of them are based on thermodynamic quantities (specific heat, isothermal compressibility, etc.). In these methods the difference in free energy $\Delta G\left(T\right)$ between the gas and the condensed phase state is usually estimated at a specific temperature.[5] While $\Delta G\left(T\right)$ is important for distinguishing between hydrophilic and hydrophobic solutes, atomistic insights are not rigorous, and the methodology is cumbersome. In addition, $\Delta G\left(T\right)$ values provide only a general picture of the system state. In fact, in this framework, thermodynamic quantities are obtained as difference between state functions and these are intrinsically prone to compensation of errors. The main limitation of a basic thermodynamic approach is that it does not take into account the shape of the potential energy surface (PES) describing the interaction between nuclei because these types of calculations are based on energy differences obtained from single point energy estimates at the bottom of the potential energy well often even in a harmonic fashion. From an atomistic point of view, these calculations provide information mainly about the molecular geometry at minima. Other techniques, based on a dynamical approach, have been developed. Among those techniques, globally known as

enhanced sampling methods, metadynamics and umbrella sampling performed along 'alchemical' collective variables, are arguably the most successful and commonly employed method to access thermodynamic information on complex system solvation.[6]

To gain atomistic insight, we choose to employ vibrational spectroscopy. This technique is able to detect the interactions that are responsible for the solvation process because it encompasses the detection of strong chemical bonds as well as long-range weak solute-solvent interactions. These include hydrogen bonding and many other intermolecular interactions originated by the surrounding molecules, such as electrostatic and polarization dispersion interactions or electronic cloud repulsion. All these information are embodied in the PES shape, and the shape of the potential can be re-conducted directly to each atomic component of the molecule, providing in this way a direct atomistic insight. Typically, modes of vibrations will experience a change in frequency when switching from the isolated molecule (gas phase) to the solvated state (solution) arrangement. For these reasons, the use of computational vibrational spectroscopy simulations through molecular dynamics methods allows to directly relate the experimental results with the interactions between the solute and the solvent molecules at atomistic level.

By means of vibrational spectroscopy, one can appreciate blue and red frequency shifts, which are related respectively to a stiffer (increase of the force constant) and floppier (decrease of the force constant) vibrational motion. More specifically, red shifts are usually originated from the weakening of the bond order, as they occur during the formation of hydrogen bonding, for example. Instead, the blue shifts are less frequent and they may be originated by increasing the bond order by adding, for example, ionic interactions on top of covalent ones. Another typical blue shift case is the one involving a bending frequency after a hydrogen bonding formation, since H-bond makes bending more difficult (i.e. stiffer) due to the directionality of the H-bond itself. These are just a few examples of interactions that can be detected by vibrational spectroscopy. Vibrational spectroscopy is more sensitive than electronic spectroscopy, where the energy range is even hundreds of times larger, and

it is more difficult to reach the same detail of description. Also, in a typical electronic spectroscopy simulation of large molecular systems, the shape of the nuclear potential is taken into account indirectly. Indeed, it is the statistical average of the electronic transition at these different nuclear arrangements to provide both the frequency values and the intensities of the simulated spectrum.[7–10] This method is the most valuable in these cases though it is not able to capture some important features of nuclear vibrational motions which can be important when studying phenomena like reactivity.

To study the effects of water solvation and provide a prototype of the quantum dynamical behavior of complex solvated systems, we choose a system for which the spectroscopic differences going from solvation by water to gas phase are evident. Thymidine fits this case very well. It is a biologically relevant molecule, and it has been experimentally characterized[11,12] in the infra-red region. More importantly for our goals, thymidine presents in the gas phase two vibrational stretching signals, one for the C4 = O stretching at 1714 cm^{-1} and another for the C5 = C6 stretching at 1662 cm^{-1}, which are degenerate at 1710 cm^{-1} in water solution (see Fig. 1c). This vibrational degeneracy is not induced by symmetry and it will provide our qualitative and quantitative accuracy check in the description of the solvation process.

Given this atomistic quantum mechanical scenario, we think that an accurate simulation aiming at reproducing the effects of water solvation should be based on *ab initio* electronic structure calculations (QM) and reproduce nuclear quantum effects by vibrational dynamics. Due to the nature of the problem, it would be desirable to apply this approach not only to the solute but also to all the solvating water molecules. Since this is not possible, in this work we adopt a QM/MM approach, where we downgrade the accuracy of the solvent, the Molecular Mechanics (MM) part, to the level of the AMOEBA force field (FF) potential to describe the water solvent.[13–16] This is expected to be still an accurate approach since previous FF-based simulations of large solvated systems showed the importance of the interaction energies in solvation,[17] and the presence of gas-to-water solvatochromic shifts.[18]

Nuclear quantum effects (NQEs) are reproduced by our Divide-and-Conquer Semiclassical Initial Value Representation (DC SCIVR) molecular dynamics method.[19–23] We think it is important to include quantum mechanical effects, especially the zero point energy one, in our molecular dynamics simulations because results on similar systems featuring strong hydrogen bonding have demonstrated that a quantum description of the nuclei was certainly needed to obtain accurate results.[24–28] Furthermore, NQEs have been observed to be important also in cases involving the motion of heavy atoms.[29–31] More specifically for our system, the presence of NQEs in small to large clusters and bulk water has been studied from different perspectives,[32] and in all cases the inclusion of quantum mechanical effects allowed to reproduce the experimental results.[33–35] In particular, in vibrational spectroscopy, two of us proved that only a quantum mechanical simulation is able to reproduce all the main experimental features of the liquid water IR spectrum, i.e. including the bending-libration combination bands.[36,37]

One of our goals is to test different solvent models using both implicit and explicit methods. This helps us not only observe which kind of potential returns the best results compared to the experiment, but it also sheds light on the nature of the interactions occurring between the solute and the solvent. The whole idea of the work is well summarized in Fig. 1, where we start from the bulk system, featuring many atoms and molecules interacting with each other (panel a). Then, using trajectory analysis with different models of solvent it is possible to understand the main sites of interactions (panel b). Finally, by analyzing the data, a clear atomistic vision of the problem is delivered (panel c).

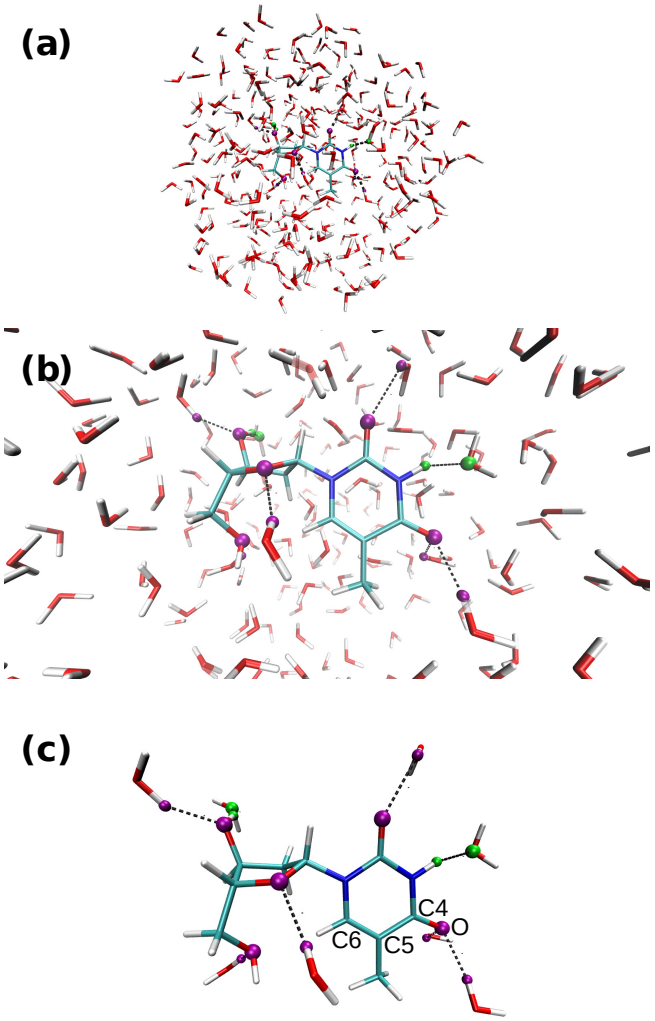

Figure 1: Atomistic representation of thymidine in water solvent. Panel (a) is the full simulated system. Panel (b) is a close up picture showing that very few molecules are directly interacting with thymidine at each time-step. Panel (c) represents the thymidine H-bonded water molecules at given time-step.

Methods

Our goal is to simulate the gas-to-water solvatochromic ν(C6=C5) and ν(C4=O) shifts of thymidine, where the atomic labels are reported in Fig.1(c). As anticipated, we employ a QM/MM interaction potential calculation scheme, where the QM subsystem is treated at the level of B3LYP/6-31G* density functional theory with Grimme dispersion corrections.[38] The MM part is composed by all the solvating water molecules and these are described by the AMOEBABIO18 force field. The QM/MM method is implemented by interfacing a modified in-house development version of Gaussian,[39] with the molecular mechanics Tinker software suite.[40–43] These atomistic simulations are composed of 974 atoms in a droplet model with a repulsive wall on the edge of the solvation sphere, as reported in Fig.1(a). There have been several QM/MM implementations proposed over the years,[44–52] mainly differing in the way the interactions between the MM and the QM parts are described. Our QM/MM approach implements the most sophisticated scheme of QM/MM embedding, known in literature as polarizable embedding. In this method, the MM part can polarize the QM subsystem and vice versa.[14,15,41] This QM/MM set-up showed encouraging results in photochemistry when applied to photoreceptive protein systems.[53,54]

A complete description of the QM/AMOEBA implementation and methods can be found in ref.[14,15] Specifically, within this framework, the total energy of the system with nuclear configuration $\mathbf{Q}$ is expressed as:

$$E(\mathbf{Q}, \mathbf{P}, \boldsymbol{\mu}_d, \boldsymbol{\mu}_p) = E_{QM}(\mathbf{Q}, \mathbf{P}) + E_{env}(\mathbf{Q}, \mathbf{P}, \boldsymbol{\mu}_d, \boldsymbol{\mu}_p) \tag{1}$$

where both the QM potential term (E_{QM}) and the MM one (E_{env}) are functionals of the system geometry ($\mathbf{Q}$) and the density matrix $\mathbf{P}$. In addition, the environment depends on two sets of $\boldsymbol{\mu}_d$ and $\boldsymbol{\mu}_p$ dipole moments, which are generated respectively by the direct electric field ($\mathbf{E}_d$) and the polarizable electric field ($\mathbf{E}_p$). The QM term (E_{QM}) is obtained through

Self Consistent Field (SCF) techniques, while E_{env} is defined as follows:

$$E_{env}(\mathbf{Q},\mathbf{P},\boldsymbol{\mu}_d,\boldsymbol{\mu}_p) = E_{FF}(\mathbf{Q}) + E_{pol}(\mathbf{Q},\mathbf{P},\boldsymbol{\mu}_d,\boldsymbol{\mu}_p) + E_{QM/MM}(\mathbf{Q},\mathbf{P}) \tag{2}$$

where E_{FF} is the sum of the classical FF terms without the electrostatic term, E_{pol} is the polarization energy, and $E_{QM/MM}$ is a coupling term between the QM and MM part containing the permanent multipoles. It is the E_{pol} term to encrypt the mutual polarization between the QM and the MM part. This term contains the definition of polarization energy as defined in AMOEBA but in a variational way.[55] The minimizers of the functional are the direct and polarization dipoles. This potential term also includes the contribution of the interaction with the QM electric field which is

$$E_{pol}(\mathbf{Q},\mathbf{P},\boldsymbol{\mu}) = \frac{1}{2}\boldsymbol{\mu}_d^T\mathcal{T}\boldsymbol{\mu}_p - \frac{1}{2}\left(\boldsymbol{\mu}_p^T\mathbf{E}_d + \boldsymbol{\mu}_d^T\mathbf{E}_p\right) - \frac{1}{2}\left(\boldsymbol{\mu}_p + \boldsymbol{\mu}_d\right)^T\mathbf{E}_{QM}(\mathbf{Q},\mathbf{P}). \tag{3}$$

Further information about the computation protocol can be found in the SI and a complete description of the QM/AMOEBA implementation and methods can be found in ref.[14,15] Our FF calculations have been carried out using AMOEBABIO18,[13,16,40] which includes the polarizability by means of a sophisticated approach exploiting a self-consistent procedure developed by Thole.[56,57] An extensive examination of the factors that led us to choose this FF as the most suitable one for vibrational spectroscopy of these systems can be found in a previous work done by two of us.[20]

This level of electronic theory and setup can be employed for vibrational spectroscopy calculations. Specifically, we calculate the vibrational ν(C6=C5) and ν(C4=O) frequencies at different levels of accuracy. The computationally cheaper method to compute vibrational frequencies is the harmonic approximation, which is obtained through Hessian diagonalization at the solvated thymidine minimum geometry. Also, it should be noted that in complex or solvated systems several almost isoenergetic minima are present and the single-minimum harmonic method shows its shortcomings. Therefore, we do not think that scaling harmonic

values by using ad-hoc factors is the best way to include anharmonicity and Nuclear Quantum Effects (NQEs).[58–61] At a higher computational level, classical anharmonicity can be taken into account by molecular dynamics (MD) approaches where multiple minima can be explored and the power spectrum is computed by Fourier Transform (FT) of the classical momentum autocorrelation function. We consider the two main classical MD methods, i.e. the one performed in the microcanonical NVE ensemble, commonly named quasi-classical trajectory (QCT)[62–66] or quasi-classical molecular dynamics method,[67,68] where the classical trajectory energy is constant, and the one performed in the canonical or NVT ensemble, where the trajectory energy is changed according to a thermostat to reproduce the Boltzmann distribution. In vibrational spectroscopy simulations where a single NVE trajectory is employed, the initial conditions are very important for a correct potential sampling.[69,70] We choose to run our trajectories starting from the thymidine minimum geometry and at the harmonic ZPE energy shell to properly account for the anharmonic part of the potential. In our NVT approach, the frequencies are still obtained as Fourier transform of the linear momentum autocorrelation function of an NVE trajectory but after a long enough NVT thermalization run at the target temperature.

One can include NQEs in addition to classical anharmonicity at higher computational cost. A pre-computed potential energy surface (PES)[71–78] is usually required and the dimensionality of the calculation is limited. To overcome this curse of dimensionality, some of us recently introduced the Multiple Coherent[79,80] (MC) Semiclassical Initial Value Representation[81] (SCIVR), which allows one to make accurate estimates of vibrational eigenvalues and eigenfunctions using a single classical trajectory, given that the energy of the trajectory is reasonably close to the exact eigenvalue.[82] The method is based on the semiclassical approximation[83–98] of the exact quantum propagator. This is particularly useful when a fitted PES is not available and the computation of the potential has to be done on the fly. Since the energy of the vibrational states is not known *a priori*, an educated guess is to run the trajectories with energy equal to the harmonic Zero Point Energy (ZPE). This semiclassical method

coupled with the recently developed Divide and Conquer[99–101] (DC) approach allowed us to compute the quantum mechanical vibrational frequencies of large systems,[20,102–104] featuring up to 10000 degrees of freedom.[105] More specifically, in the DC-SCIVR method, the vibrational spectrum is divided into subspaces and all the classical dynamics quantities, obtained from the full dimensional trajectory, necessary to the calculation of the nuclear power spectrum are projected into each subspace. The final MC-DC-SCIVR formulation of the quantum mechanical power spectrum using a single trajectory is the following

$$\tilde{I}(E) = \left(\frac{1}{2\pi\hbar}\right)^{Nvib} \frac{1}{2\pi\hbar T} \left| \int_0^T e^{\frac{i}{\hbar}\left[\tilde{S}_t\left(\tilde{\mathbf{p}}_0,\tilde{\mathbf{q}}_0\right)+Et+\tilde{\phi}_t\left(\tilde{\mathbf{p}}_0,\tilde{\mathbf{q}}_0\right)\right]} \langle\tilde{\Psi}\big|\tilde{\mathbf{p}}_t,\tilde{\mathbf{q}}_t\rangle \, dt \right|^2 , \tag{4}$$

where $\tilde{S}_t$ is the approximate projected classical action of the classical trajectory generated with initial conditions $\left(\tilde{\mathbf{p}}_0,\tilde{\mathbf{q}}_0\right)$. $\tilde{\phi}_t$ is the phase of the Herman-Kluck prefactor,[84–87] and $\langle\tilde{\Psi}\big|\tilde{\mathbf{p}}_t,\tilde{\mathbf{q}}_t\rangle$ is the overlap between the coherent state centered at phase space point $\left(\tilde{\mathbf{p}}_t,\tilde{\mathbf{q}}_t\right)$ and a reference state. Further information about our semiclassical methods can be found in the Supporting Information.

Results

We start by simulating the system in Fig.1(c) using a FF description for both thymidine and water. We employ classical MD with AMOEBA FF following both NVE and NVT procedures, and compare these results with the experiment, as reported in Fig.(2). Both the experiment and the NVT simulation are at 300 K.

The vertical dashed lines in Fig.(2) represent the harmonic approximation for the two stretch frequencies and their Mean Absolute Error (MAE) is 70 cm^{-1}, which is quite off the mark compared to the experimental values where the C5=C6 and C4=O stretching frequency are degenerate,[12] as obtained also from an extensive isotopic labeling experiment.[106] More importantly, the harmonic approximation cannot reproduce the mode degeneracy, as there is a frequency gap between the two modes (Δ) equals to 45 cm^{-1}. One would expect a

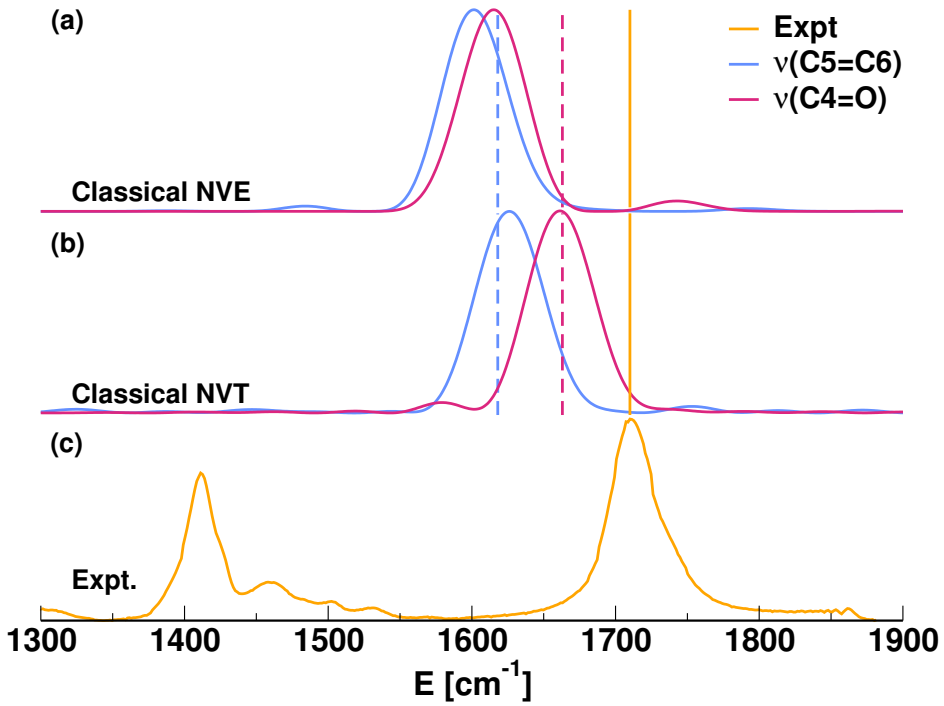

Figure 2: Classical NVE (panel a) and NVT (panel b) MD spectra of the water-solvated thymidine molecule for the C5=C6 and the C4=O bond stretching motions using AMOEBA FF. Vertical dashed lines are the harmonic estimates. The mustard-colored spectrum (panel c) is the experiment where the C5=C6 and C4=O stretching frequency are degenerate.[106] The experimental peak at $\approx 1400\,\mathrm{cm}^{-1}$ is not related to the C5=C6 and C4=O signals under investigation.

better MAE by adding anharmonicity through the NVE simulation. Instead, the accuracy is worse than in the harmonic case. This is probably due to the fact that the force field is parametrized in a way that the harmonic estimate is not a pure one, but it already implicitly includes a certain level of anharmonicity and red shift. When performing the NVE simulation we take this into account again, and the red shift is increased.

However, the NVE simulation closes the gap between the two mode frequencies ($\Delta = 13\ \mathrm{cm}^{-1}$) getting a picture which is similar to the experimental one. This first comparison is suggesting that the FF is qualitatively accurate since it mimics the right trend, but not quantitative. In the middle panel of Fig.(2) we report the NVT classical power spectrum at the experimental temperature. This simulation essentially fails to go beyond the harmonic approximation. This clearly indicates that the NVT single trajectory protocol at room temperature does not sample enough the anharmonic potential energy region. Instead, a single trajectory run at the ZPE energy is able to catch the anharmonicities of the system, as shown in the NVE simulation.

Thus, we need to move to a more accurate potential representation using the QM/MM method, where thymidine is at the DFT level and the solvent is described with FF accuracy, as detailed above. Previous simulations on similar systems are encouraging and showed that the DFT level of theory is enough for getting accurate vibrational frequencies.[20,103,105]

When we apply our QM/MM semiclassical (DC-SCIVR and DFT/AMOEBA) scheme to the explicitly solvated thymidine system of Fig. 1(c), we obtain the power spectra reported in Figure 3. Specifically, in panel (a) of Fig.(3) we show the convolution of the ν(C5=C6) and ν(C4=O) simulated signals to be compared with the experimental one reported in panel (c) of Fig.(3). In this case, the frequency value is very accurate compared to experimental signal ($1700\ \mathrm{cm}^{-1}$ *vs* $1710\ \mathrm{cm}^{-1}$) and our simulated bandwidth at half maximum is about $70\ \mathrm{cm}^{-1}$ compared to about $45\ \mathrm{cm}^{-1}$ of the experiment. The larger width is mainly due to the facts that our method employs a Fourier transform of a short, finite-time evolution and that we are simulating a power spectrum, so other quantum mechanical transitions different

from the fundamental ones, but coupled to them, may contribute to increase the width of the computed band. We did not want to spoil our time-dependent calculations, which provide a physically-based bandwidth, using unphysical filtering or Lorentzian fittings. We can better appreciate how our semiclassical QM/MM mimics the correct physics of solvation by looking at panel (b) of Fig.(3), where thymidine ν(C5=C6) and ν(C4=O) signals are reported separately both in gas-phase (dashed line) and in the solvated system (continuous line). DC-SCIVR DFT/AMOEBA shows that in water the Mean Absolute Error (MAE) from the experiment is only 15 cm^{-1}, and the frequency gap is greatly reduced (Δ = 12 cm^{-1}). Overall, these results represent a significant improvement in terms of accuracy compared to the full FF approach.

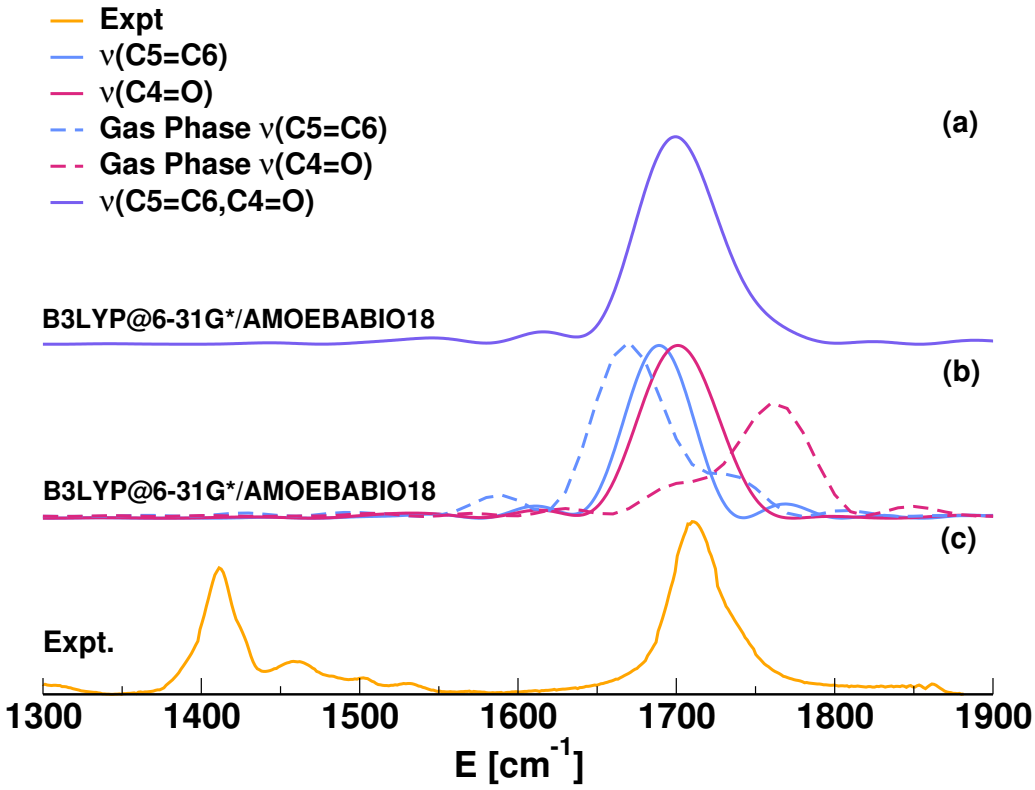

Figure 3: Semiclassical (DC SCIVR) QM/MM power spectra for the C5=C6 and C4=O bond stretches of water-solvated thymidine. QM at DFT-B3LYP/6-31G* level of theory and MM at the level of AMOEBABIO18. Panel (a): The convoluted ν(C4=O) and ν(C5=C6) simulated signal. Panel (b): The separated ν(C4=O) and ν(C5=C6) signals for gas-phase (dashed lines) and water solvated (continuous line) thymidine. Panel (c): The mustard-colored experimental spectrum showing a degeneracy of the two C5=C6 and C4=O stretch frequencies at 1710 cm^{-1}.

We now try to understand how the different interactions at play influence the accuracy of the simulation, and what the peculiar properties of water solvation are. We achieve these goals by checking different models for the MM potential. We start from the TIP3P water model,[107] in which the potential energy of every molecule is represented by a harmonic bond and angle term. Non-bonding interactions are modeled by punctual charges placed on the atomic positions, and the van der Waals (VDW) interactions are accounted for by a 12-6 Lennard-Jonnes (LJ) potential. The spectrum is reported on panel (a) of Fig. (4). The limited flexibility and the lack of polarization of this model potential is causing the opposite effects of water solvation. The ν(C4=O) stretching frequency is blue-shifted at almost 1800 cm^{-1} while the ν(C5=C6) signal cannot be easily identified. In a second method, we significantly increase the quality of the description of intermolecular interactions, and the potential energy of water molecules is modeled by means of the AMOEBA FF. This means that anharmonic stretching and bending terms are considered together with atomic multipoles up to the quadrupole. In addition, 1,3 intermolecular interactions are modeled by the Urey-Bradley potential,[108] and the VdW interactions have a functional form similar to the LJ potential. Here, however, we have switched off the polarization parameters. This means that the MM subsystem cannot be polarized by the QM. This case is reported in panel (b) of Fig. 4 where the ν(C4=O) stretch frequency is red-shifted by a small amount with respect to the gas phase, i.e. up to 1750 cm^{-1}. The ν(C5=C6) frequency is left invariant compared to the gas-phase signal and no blue shift solvation effect is reproduced. In this case, the MAE (44 cm^{-1}) and the Δ parameter (88 cm^{-1}) are far away from the correct physical description of the solvation process. Finally, in a third approach the solvent is represented as a continuum according to the Polarizable Continuum Model (PCM).[7,109–114] This case is reported in panel (c) of Fig.(4) and the accuracy is comparable to our best QM/MM result with a MAE of (5 cm^{-1}) and a Δ of (10 cm^{-1}). This definitely proves that it is the reciprocal polarization between the solute and the solvent to mainly characterize water solvation peculiarities. In fact, this implicit model of solvation mainly focuses on

reproducing the electrostatic and polarization effects that the solvent exerts on the central molecule and vice versa.

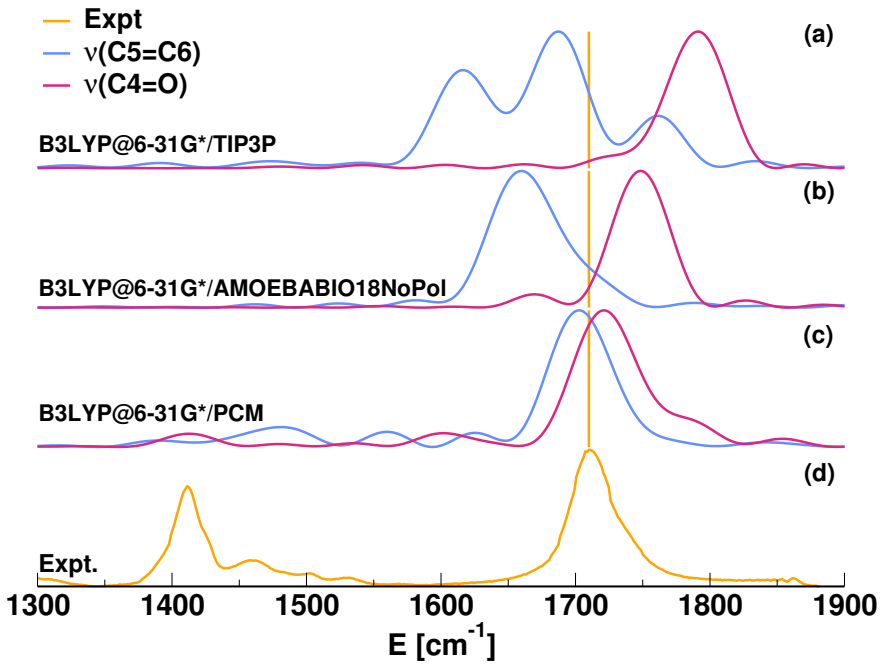

Figure 4: Semiclassical power spectra for the ν (C4=O) and ν (C5=C6) stretch signals. Panel (a) refers to the QM/TIP3P solvent model. Panel (b) refers to the QM/AMOEBABIO18 scheme without polarization, and panel (c) refers to the PCM implicit model of the solvent. Panel (d) is the experimental spectrum.

Discussion

The results suggest that the issue of deciphering the nature of solute-water solvent interaction is a challenging one, and that only accurate spectroscopic techniques can detect the roles of classical and quantum contributions. The classical-like terms are those of the type of electrostatic interactions, while the exclusively quantum interactions are mainly electron cloud repulsion and nuclear zero-point energy effects. More specifically, the accuracy of the PCM approach shows that the polarization and the consequent electrostatic interactions are essential to reproduce the mechanics of water solvation. This is confirmed by the fact that no significant difference in the ν (C5=C6) and ν (C=O) frequencies is observed in $N, N -$

DMF solution compared to the gas-phase one.[12] We also performed a search for directional interactions along the QM/AMOEBA trajectory with the central thymidine molecule playing both as a donor and an acceptor. No substantial and strong directional interactions were found (a more detailed analysis can be found in Figure S1 of the SI). Therefore, we conclude that, in this particular case, the PCM results are accurate as the polarization interactions are mainly isotropic. The agreement of our drop model with PCM proves also that we did properly account for the long-range polarization effects of the bulk.

Moving to the atomistic details, our simulation allows us to appreciate how the blue-shift of the ν(C5=C6) value is mainly due to the presence of electron cloud repulsions during the quantum molecular dynamics motion, which causes the C5=C6 potential interaction to be stiffer compared to the gas phase one. In other words the natural packing present in the liquid phase is at the origin of the blue-shift of the ν(C5=C6) stretch. This is not only a steric matter but also a quantum mechanical one, since large amplitude vibrations in solution would cause the electronic clouds to partially overlap. To quantify this consideration, we employ the symmetry-adapted intermolecular perturbation theory (SAPT)[115] with the MOLPRO suite of packages[116] for the calculation of the electronic exchange energy between molecular fragments. In our case one fragment is represented by the entire thymidine molecule, and the other by the water molecules nearest to thymidine, as reported in the left panel of Fig. 5. Specifically, it is an H-atom interacting with the thymidine C=O group, which is the nearest point of contact between fragments (dotted line in the left panel of Fig. 5). Considering that this atom is vibrating much faster than the rate at which the two molecules (thymidine and water) are adjusting, we calculate the one-dimensional potential reported on the right panel of Fig. 5. This potential is anharmonic and differs from a Morse (blu line) or harmonic (red line) approximation. Using sinc-DVR,[117,118] we calculate the exact one-dimensional ground state vibrational eigenvalue and eigenfunction for these potentials and the quantum delocalization (gray shadow region) of the proton from the quantum root mean squared displacement evaluation, also reported in the left panel. The SAPT allows us to estimate

the exchange energy between fragments, also denoted as Pauli repulsion, as the sum of three contributions of different type and order, i.e $E_{exch} = E^{(1)}_{exch} + E^{(2)}_{exch-ind} + E^{(2)}_{exch-disp}$, where *ind* and *disp* stands respectively for "induction" and "dispersion". The values of exchange energy are reported on the Table on the right panel of Fig. 5 for the different geometries just described, i.e. the starting equilibrium geometry ("Equilibrium"), the geometry at which the water molecule is the nearest to thymidine ("Stretched") and those obtained by the quantum proton delocalization. We find that the stretched molecular dynamics simulation geometry

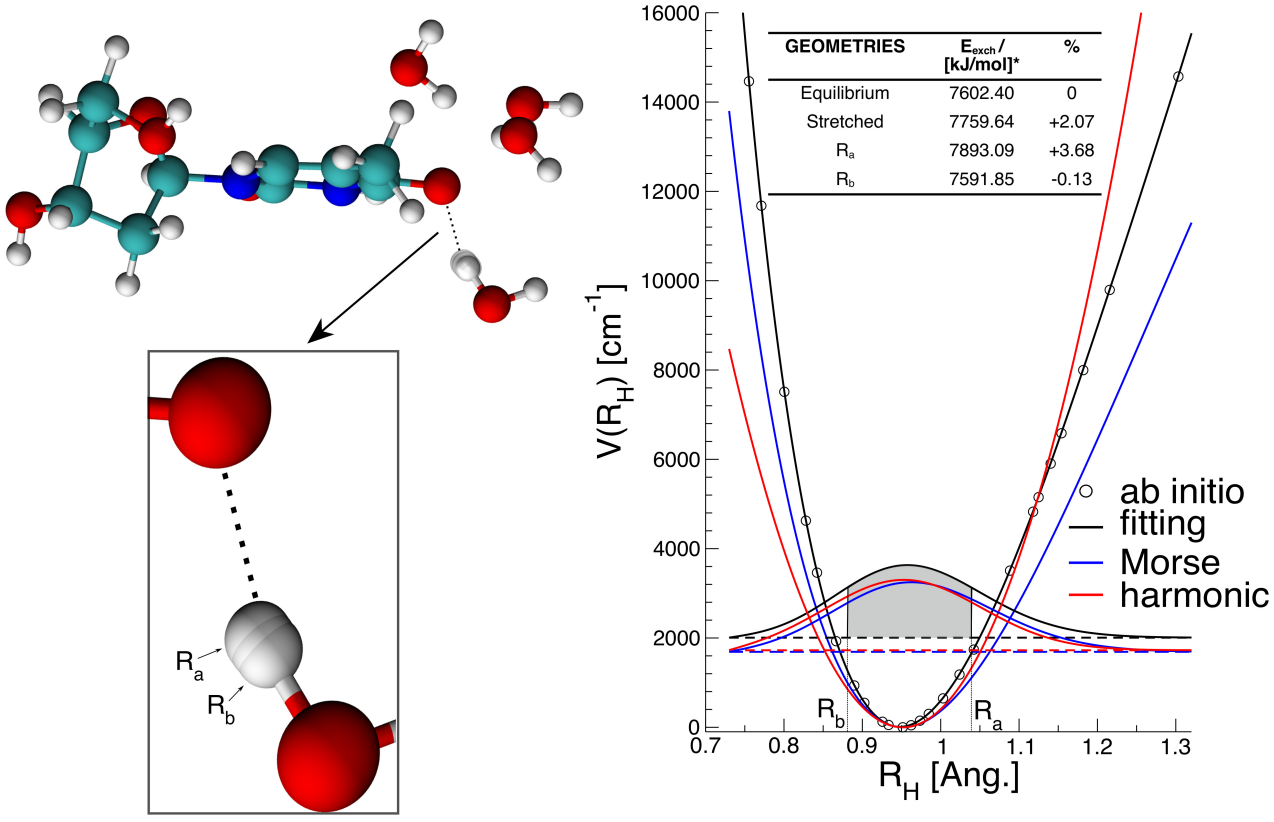

Figure 5: Thymidine atomic solvation interactions. Left panel shows a molecular dynamics snap-shot with the most interacting, i.e. the nearest, water molecules. The water H-atom interacting with the thymidine C=O group is highlighted. Right panel shows the one-dimensional potential energy experienced by the highlighted H-atom at different approximations, together with the exact ground vibrational eigenfunction. The root mean squared displacement is the shadow area. Upper right Table: The ab initio exchange electronic energy contribution for different geometries together with the percentage variation with respect to the equilibrium geometry.

is experiencing a +2.1% increment in electronic repulsion over the total contribution coming

from all the electrons of the fragments, and this is mainly originated from the interacting H-atom. With the inclusion of the quantum H-atom delocalization the repulsion is raised at almost +3.8%. We deem this increment to be significant in electronic structure theory, since it is due to the delocalization of a single atom only. Thus, we conclude that, even if the water molecules are not directly interacting with the C=C stretch, it is this type of interaction together with the dynamical coupling of the water solvent to be responsible for the C=C blue shift.

Clearly, this electronic steric issue is somehow true for any kind of stretches of the solvated molecule, since there is less room for vibration in water solution than in the gas phase. However, for the ν(C4=O) stretch, a red-shift is prevailing because of the interplay of other electrostatic interactions. In this regard, it is interesting to look at the Radial Distribution Function (RDF) associated to our NVE trajectory reported in the SI, Fig.S1. It is possible to see how in the TIP3P water model, the packing is greatly reduced with respect to the AMOEBA FF more precisely by an amount greater than 1Å. We think that this observation explains not only the larger frequency gap, which is about the same as in gas phase, but also the wrong sign of the shift of the ν(C4=O). The packing is also reduced for the FF when the polarization is removed, but for a fewer amount ($\sim$ 0.4Å). This could explain the smaller amount of both red- and blue- shifts observed with this computational set-up. Instead, in the full QM/AMOEBA computational set-up of panel (b) of Fig. 3, we account for the mutual polarization of the MM and QM portions, showing that it plays a crucial role in aqueous systems. Specifically, what makes the difference between the accurate results of panel (b) of Fig. 3 and those of panel (b) of Fig. 4 is the fact that to reach accuracy we have to explicitly set-up a so-called polarizable embedding (PE) scheme where the MM force field contains additional terms accounting for the polarization effects induced by the QM density.

Conclusions

In the present work, we have shown that the QM/MM Semiclassical method can reach spectroscopic accuracy in the calculation of IR (and Raman) frequencies of biological molecules in water solution. Specifically, by means of our DC- SCIVR quantum dynamics approach coupled with a polarizable QM/MM representation of the PES, we were able to get very close to the degeneracy of the thymidine ν(C4=O) and ν(C5=C6) stretch signals typical of water solution, and showed that indeed quantum effects and anharmonicities play an important role in determining the dynamical behaviour and the spectroscopic features of water solvated molecules.

We were able to indirectly detect the net electronic cloud repulsion effects when performing nuclear quantum dynamics. This shows that the dynamics of biomolecules in water solution experiences not only H-bonds, multipoles, and short and long range polarization interactions but also packing effects. These effects are originated from the fact that there is fewer room for the nuclear wavepacket to vibrate given the electronic clouds superpositions and this explains the observed spectroscopic blue-shift.

Author Contributions

(D.M. and G.M.) These authors contributed equally.

Acknowledgement

M.C. acknowledges financial support from the European Research Council (Grant Agreement No. (647107)—SEMICOMPLEX—ERC-2014-CoG under the European Union's Horizon 2020 and No. 101081361 — SEMISOFT — ERC-2022-POC2 under Horizon Europe research and innovation programme). D.M. and G.M. acknowledges the University of Milan for their Ph.D. scholarships. M.B. and B.M. acknowledges financial support from the European

Research Council (Grant Agreement No. (786714)—LIFETIMES—ERC-2017-ADG).

Supporting Information Available

The Supporting Information file includes: additional details about the semiclassical theory employed; computational details about optimizations, employed trajectories, and frequencies of vibration; analysis of trajectories and radial distribution functions.

References

(1) Bellissent-Funel, M.-C.; Hassanali, A.; Havenith, M.; Henchman, R.; Pohl, P.; Sterpone, F.; van der Spoel, D.; Xu, Y.; Garcia, A. E. Water Determines the Structure and Dynamics of Proteins. *Chem. Rev.* **2016**, *116*, 7673–7697, PMID: 27186992.

(2) Czajka, D. M.; Finkel, A. J.; Fischer, C. S.; Katz, J. J. Physiological effects of deuterium on dogs. *Am. J. Physiology-Legacy Cont.* **1961**, *201*, 357–362, PMID: 13719048.

(3) Levinson, N. M.; Fried, S. D.; Boxer, S. G. Solvent-Induced Infrared Frequency Shifts in Aromatic Nitriles Are Quantitatively Described by the Vibrational Stark Effect. *J. Phys. Chem. B* **2012**, *116*, 10470–10476, PMID: 22448878.

(4) Schleif, T.; Prado Merini, M.; Henkel, S.; Sander, W. Solvation Effects on Quantum Tunneling Reactions. *Acc. Chem. Res.* **2022**, *55*, 2180–2190, PMID: 35730754.

(5) Cramer, C. J.; Truhlar, D. G. A universal approach to solvation modeling. *Acc. Chem. Res.* **2008**, *41*, 760–768.

(6) Wu, P.; Hu, X.; Yang, W. λ-metadynamics approach to compute absolute solvation free energy. *J. Phys. Chem. Lett.* **2011**, *2*, 2099–2103.

(7) Lipparini, F.; Scalmani, G.; Mennucci, B.; Cances, E.; Caricato, M.; Frisch, M. J. A variational formulation of the polarizable continuum model. *J. Chem. Phys.* **2010**, *133*, 014106.

(8) Mennucci, B. Continuum solvation models: What else can we learn from them? *J. Phys. Chem. Lett.* **2010**, *1*, 1666–1674.

(9) Giovannini, T.; Egidi, F.; Cappelli, C. Molecular spectroscopy of aqueous solutions: a theoretical perspective. *Chem. Soc. Rev.* **2020**, *49*, 5664–5677.

(10) Giovannini, T.; Cappelli, C. Continuum vs. atomistic approaches to computational spectroscopy of solvated systems. *Chem. Commun.* **2023**, *59*, 5644–5660.

(11) Ivanov, A. Y.; Stepanian, S.; Karachevtsev, V.; Adamowicz, L. Nucleoside conformers in low-temperature argon matrices: Fourier transform IR spectroscopy of isolated thymidine and deuterothymidine molecules and quantum-mechanical calculations. *Low Temp. Phys.* **2019**, *45*, 1008–1017.

(12) Beyere, L.; Arboleda, P.; Monga, V.; Loppnow, G. The dependence of thymine and thymidine Raman spectra on solvent. *Can. J. Chem.* **2004**, *82*, 1092–1101.

(13) Ponder, J. W.; Wu, C.; Ren, P.; Pande, V. S.; Chodera, J. D.; Schnieders, M. J.; Haque, I.; Mobley, D. L.; Lambrecht, D. S.; DiStasio Jr, R. A., et al. Current status of the AMOEBA polarizable force field. *J. Phys. Chem. B* **2010**, *114*, 2549–2564.

(14) Loco, D.; Polack, E.; Caprasecca, S.; Lagardère, L.; Lipparini, F.; Piquemal, J.-P.; Mennucci, B. A QM/MM Approach Using the AMOEBA Polarizable Embedding: From Ground State Energies to Electronic Excitations. *J. Chem. Theory Comput.* **2016**, *12*, 3654–3661, PMID: 27340904.

(15) Loco, D.; Lagardere, L.; Caprasecca, S.; Lipparini, F.; Mennucci, B.; Piquemal, J.-

P. Hybrid QM/MM Molecular Dynamics with AMOEBA Polarizable Embedding. *J. Chem. Theory Comput.* **2017**, *13*, 4025–4033, PMID: 28759205.

(16) Shi, Y.; Xia, Z.; Zhang, J.; Best, R.; Wu, C.; Ponder, J. W.; Ren, P. Polarizable atomic multipole-based AMOEBA force field for proteins. *J. Chem. Theory Comput.* **2013**, *9*, 4046–4063.

(17) Stöhr, M.; Tkatchenko, A. Quantum mechanics of proteins in explicit water: The role of plasmon-like solute-solvent interactions. *Sci. Adv.* **2019**, *5*, eaax0024.

(18) Homem-de Mello, P.; Mennucci, B.; Tomasi, J.; Da Silva, A. The effects of solvation in the theoretical spectra of cationic dyes. *Theor. Chem. Acc.* **2005**, *113*, 274–280.

(19) Aieta, C.; Micciarelli, M.; Bertaina, G.; Ceotto, M. Anharmonic quantum nuclear densities from full dimensional vibrational eigenfunctions with application to protonated glycine. *Nat. Commun.* **2020**, *11*, 4348.

(20) Gabas, F.; Conte, R.; Ceotto, M. Semiclassical vibrational spectroscopy of biological molecules using force fields. *J. Chem. Theory Comput.* **2020**, *16*, 3476–3485.

(21) Reduced rovibrational coupling Cartesian dynamics for semiclassical calculations: Application to the spectrum of the Zundel cation. *J. Chem. Phys.* **2019**, *151*.

(22) Botti, G.; Ceotto, M.; Conte, R. On-the-fly adiabatically switched semiclassical initial value representation molecular dynamics for vibrational spectroscopy of biomolecules. *J. Chem. Phys.* **2021**, *155*.

(23) Schwaab, G.; de Tudela, R. P.; Mani, D.; Pal, N.; Roy, T. K.; Gabas, F.; Conte, R.; Caballero, L. D.; Ceotto, M.; Marx, D., et al. Zwitter ionization of glycine at outer space conditions due to microhydration by six water molecules. *Phys. Rev. Lett.* **2022**, *128*, 033001.

(24) Klinman, J. P.; Kohen, A. Hydrogen tunneling links protein dynamics to enzyme catalysis. *Ann. Rev. Biochem.* **2013**, *82*, 471–496.

(25) Wang, L.; Fried, S. D.; Boxer, S. G.; Markland, T. E. Quantum delocalization of protons in the hydrogen-bond network of an enzyme active site. *Proc. Natl Acad. Sci.* **2014**, *111*, 18454–18459.

(26) Pérez, A.; Tuckerman, M. E.; Hjalmarson, H. P.; Von Lilienfeld, O. A. Enol tautomers of Watson- Crick base pair models are metastable because of nuclear quantum effects. *J. Am. Chem. Soc.* **2010**, *132*, 11510–11515.

(27) Fang, W.; Chen, J.; Rossi, M.; Feng, Y.; Li, X.-Z.; Michaelides, A. Inverse temperature dependence of nuclear quantum effects in dna base pairs. *J. Phys. Chem. Lett.* **2016**, *7*, 2125–2131.

(28) Nandi, A.; Laude, G.; Khire, S. S.; Gurav, N. D.; Qu, C.; Conte, R.; Yu, Q.; Li, S.; Houston, P. L.; Gadre, S. R., et al. Ring-Polymer Instanton Tunneling Splittings of Tropolone and Isotopomers using a Δ-Machine Learned CCSD (T) Potential: Theory and Experiment Shake Hands. *Journal of the American Chemical Society* **2023**, *145*, 9655–9664.

(29) Meisner, J.; Kästner, J. Atom tunneling in chemistry. *Angew. Chemie Intl Ed.* **2016**, *55*, 5400–5413.

(30) Castro, C.; Karney, W. L. Heavy-Atom Tunneling in Organic Reactions. *Angew. Chemie* **2020**, *132*, 8431–8442.

(31) Mandelli, G.; Aieta, C.; Ceotto, M. Heavy Atom Tunneling in Organic Reactions at Coupled Cluster Potential Accuracy with a Parallel Implementation of Anharmonic Constant Calculations and Semiclassical Transition State Theory. *J. Chem. Theory Comput.* **2022**, *18*, 623–637.

(32) Marx, D.; Tuckerman, M. E.; Hutter, J.; Parrinello, M. The nature of the hydrated excess proton in water. *Nature* **1999**, *397*, 601–604.

(33) Yu, Q.; Qu, C.; Houston, P. L.; Conte, R.; Nandi, A.; Bowman, J. M. q-AQUA: A Many-Body CCSD(T) Water Potential, Including Four-Body Interactions, Demonstrates the Quantum Nature of Water from Clusters to the Liquid Phase. *J. Phys. Chem. Lett.* **2022**, *13*, 5068–5074, PMID: 35652912.

(34) Qu, C.; Yu, Q.; Houston, P. L.; Conte, R.; Nandi, A.; Bowman, J. M. Interfacing q-AQUA with a Polarizable Force Field: The Best of Both Worlds. *Journal of Chemical Theory and Computation* **2023**, *19*, 3446–3459, PMID: 37249502.

(35) Zhu, X.; Riera, M.; Bull-Vulpe, E. F.; Paesani, F. MB-pol(2023): Sub-chemical Accuracy for Water Simulations from the Gas to the Liquid Phase. *Journal of Chemical Theory and Computation* **2023**, *19*, 3551–3566.

(36) Rognoni, A.; Conte, R.; Ceotto, M. Caldeira-Leggett model vs ab initio potential: A vibrational spectroscopy test of water solvation. *J. Chem. Phys.* **2021**, *154*, 094106.

(37) Rognoni, A.; Conte, R.; Ceotto, M. How many water molecules are needed to solvate one? *Chem. Sci.* **2021**, *12*, 2060–2064.

(38) Ehrlich, S.; Moellmann, J.; Reckien, W.; Bredow, T.; Grimme, S. System-dependent dispersion coefficients for the DFT-D3 treatment of adsorption processes on ionic surfaces. *Chem. Phys. Chem.* **2011**, *12*, 3414–3420.

(39) Frisch, M. e.; Trucks, G.; Schlegel, H. B.; Scuseria, G.; Robb, M.; Cheeseman, J.; Scalmani, G.; Barone, V.; Petersson, G.; Nakatsuji, H., et al. Gaussian 16. 2016.

(40) Rackers, J. A.; Wang, Z.; Lu, C.; Laury, M. L.; Lagardère, L.; Schnieders, M. J.; Piquemal, J.-P.; Ren, P.; Ponder, J. W. Tinker 8: software tools for molecular design. *J. Chem. Theory Comput.* **2018**, *14*, 5273–5289.

(41) Bondanza, M.; Nottoli, M.; Cupellini, L.; Lipparini, F.; Mennucci, B. Polarizable embedding QM/MM: the future gold standard for complex (bio)systems? *Phys. Chem. Chem. Phys.* **2020**, *22*, 14433–14448.

(42) Lipparini, F. General Linear Scaling Implementation of Polarizable Embedding Schemes. *J. Chem. Theory Comput.* **2019**, *15*, 4312–4317.

(43) Nottoli, M.; Bondanza, M.; Mazzeo, P.; Cupellini, L.; Curutchet, C.; Loco, D.; LagardÃšre, L.; Piquemal, J.-P.; Mennucci, B.; Lipparini, F. QM/AMOEBA description of properties and dynamics of embedded molecules. *WIREs Comput. Mol. Sci. n/a*, e1674.

(44) Lin, H.; Truhlar, D. G. QM/MM: what have we learned, where are we, and where do we go from here? *Theor. Chem. Acc.* **2007**, *117*, 185–199.

(45) van der Kamp, M. W.; Mulholland, A. J. Combined quantum mechanics/molecular mechanics (QM/MM) methods in computational enzymology. *Biochem.* **2013**, *52*, 2708–2728.

(46) Brunk, E.; Rothlisberger, U. Mixed quantum mechanical/molecular mechanical molecular dynamics simulations of biological systems in ground and electronically excited states. *Chem. Rev.* **2015**, *115*, 6217–6263.

(47) Morzan, U. N.; Alonso de Armino, D. J.; Foglia, N. O.; Ramirez, F.; Gonzalez Lebrero, M. C.; Scherlis, D. A.; Estrin, D. A. Spectroscopy in complex environments from QM–MM simulations. *Chem. Rev.* **2018**, *118*, 4071–4113.

(48) Thompson, M. A. QM/MMpol: A consistent model for solute/solvent polarization. Application to the aqueous solvation and spectroscopy of formaldehyde, acetaldehyde, and acetone. *J. Phys. Chem.* **1996**, *100*, 14492–14507.

(49) Gagliardi, L.; Lindh, R.; Karlström, G. Local properties of quantum chemical systems: The LoProp approach. *J. Chem. Phys.* **2004**, *121*, 4494–4500.

(50) Soderhjelm, P.; Husberg, C.; Strambi, A.; Olivucci, M.; Ryde, U. Protein influence on electronic spectra modeled by multipoles and polarizabilities. *J. Chem. Theory Comput.* **2009**, *5*, 649–658.

(51) Olsen, J. M.; Aidas, K.; Kongsted, J. Excited States in Solution through Polarizable Embedding. *J. Chem. Theory Comput.* **2010**, *6*, 3721–3734.

(52) Sneskov, K.; Schwabe, T.; Kongsted, J.; Christiansen, O. The polarizable embedding coupled cluster method. *J. Chem. Phys.* **2011**, *134*, 104108.

(53) Macaluso, V.; Hashem, S.; Nottoli, M.; Lipparini, F.; Cupellini, L.; Mennucci, B. Ultrafast Transient Infrared Spectroscopy of Photoreceptors with Polarizable QM/MM Dynamics. *J. Phys. Chem. B* **2021**, *125*, 10282–10292, PMID: 34476939.

(54) Salvadori, G.; Macaluso, V.; Pellicci, G.; Cupellini, L.; Granucci, G.; Mennucci, B. Protein control of photochemistry and transient intermediates in phytochromes. *Nat. Commun.* **2022**, *13*, 6838.

(55) Nottoli, M.; Lipparini, F. General formulation of polarizable embedding models and of their coupling. *J. Chem. Phys.* **2020**, *153*, 224108.

(56) Thole, B. T. Molecular polarizabilities calculated with a modified dipole interaction. *Chem. Phys.* **1981**, *59*, 341–350.

(57) Van Duijnen, P. T.; Swart, M. Molecular and atomic polarizabilities: Thole's model revisited. *J. Phys. Chem. A* **1998**, *102*, 2399–2407.

(58) Gabas, F.; Di Liberto, G.; Conte, R.; Ceotto, M. Protonated glycine supramolecular systems: the need for quantum dynamics. *Chem. Sci.* **2018**, *9*, 7894–7901.

(59) Oh, H.-B.; Lin, C.; Hwang, H. Y.; Zhai, H.; Breuker, K.; Zabrouskov, V.; Carpenter, B. K.; McLafferty, F. W. Infrared photodissociation spectroscopy of electrosprayed ions in a Fourier transform mass spectrometer. *J. Am. Chem. Soc.* **2005**, *127*, 4076–4083.

(60) Wu, R.; McMahon, T. B. Infrared multiple photon dissociation spectra of proline and glycine proton-bound homodimers. Evidence for zwitterionic structure. *J. Am. Chem. Soc.* **2007**, *129*, 4864–4865.

(61) Scott, A. P.; Radom, L. Harmonic vibrational frequencies: an evaluation of Hartree-Fock, Møller- Plesset, quadratic configuration interaction, density functional theory, and semiempirical scale factors. *J. Phys. Chem.* **1996**, *100*, 16502–16513.

(62) Van-Oanh, N.-T.; Falvo, C.; Calvo, F.; Lauvergnat, D.; Basire, M.; Gaigeot, M.-P.; Parneix, P. Improving anharmonic infrared spectra using semiclassically prepared molecular dynamics simulations. *Physi. Chem. Chem. Phys.* **2012**, *14*, 2381–2390.

(63) Barbiero, D.; Bertaina, G.; Ceotto, M.; Conte, R. Anharmonic Assignment of the Water Octamer Spectrum in the OH Stretch Region. *J. Phys. Chem. A* **2023**, *127*, 6213–6221.

(64) Qu, C.; Bowman, J. M. IR spectra of (HCOOH) 2 and (DCOOH) 2: Experiment, VSCF/VCI, and ab initio molecular dynamics calculations using full-dimensional potential and dipole moment surfaces. *J. Phys. Chem. Lett.* **2018**, *9*, 2604–2610.

(65) Esser, T. K.; Knorke, H.; Asmis, K. R.; Schollkopf, W.; Yu, Q.; Qu, C.; Bowman, J. M.; Kaledin, M. Deconstructing prominent bands in the terahertz spectra of H7O3+ and H9O4+: Intermolecular modes in Eigen clusters. *J. Phys. Chem. Lett.* **2018**, *9*, 798–803.

(66) Fischer, T. L.; Bödecker, M.; Schweer, S. M.; Dupont, J.; Lepère, V.; Zehnacker-Rentien, A.; Suhm, M. A.; Schröder, B.; Henkes, T.; Andrada, D. M., et al. The first

HyDRA challenge for computational vibrational spectroscopy. *Phys. Chem. Chem. Phys.* **2023**, *25*, 22089–22102.

(67) Qu, C.; Bowman, J. M. IR spectra of (HCOOH) 2 and (DCOOH) 2: Experiment, VSCF/VCI, and ab initio molecular dynamics calculations using full-dimensional potential and dipole moment surfaces. *J. Phys. Chem. Lett.* **2018**, *9*, 2604–2610.

(68) Esser, T. K.; Knorke, H.; Asmis, K. R.; Schollkopf, W.; Yu, Q.; Qu, C.; Bowman, J. M.; Kaledin, M. Deconstructing prominent bands in the terahertz spectra of H7O3+ and H9O4+: Intermolecular modes in Eigen clusters. *J. Phys. Chem. Lett.* **2018**, *9*, 798–803.

(69) Conte, R.; Aieta, C.; Botti, G.; Cazzaniga, M.; Gandolfi, M.; Lanzi, C.; Mandelli, G.; Moscato, D.; Ceotto, M. Anharmonicity and quantum nuclear effects in theoretical vibrational spectroscopy: a molecular tale of two cities. *Theor. Chem. Acc.* **2023**, *142*, 1–11.

(70) Chen, Z.; Yang, Y. Incorporating Nuclear Quantum Effects in Molecular Dynamics with a Constrained Minimized Energy Surface. *J. Phys. Chem. Lett.* **2023**, *14*, 279–286.

(71) Bacic, Z.; Light, J. Highly excited vibrational levels of "floppy" triatomic molecules: A discrete variable representation Distributed Gaussian basis approach. *J. Chem. Phys.* **1986**, *85*, 4594–4604.

(72) Bacic, Z.; Light, J. C. Theoretical methods for rovibrational states of floppy molecules. *Ann. Rev. Phys. Chem.* **1989**, *40*, 469–498.

(73) Romanowski, H.; Bowman, J. POLYMODE (QCPE 496). *QCPE Bull* **1985**, *5*, 64.

(74) Bowman, J. M. The self-consistent-field approach to polyatomic vibrations. *Acc. Chem. Res.* **1986**, *19*, 202–208.

(75) Norris, L. S.; Ratner, M. A.; Roitberg, A. E.; Gerber, R. Moller–Plesset perturbation theory applied to vibrational problems. *J. Chem. Phys.* **1996**, *105*, 11261–11267.

(76) Meyer, H.-D.; Manthe, U.; Cederbaum, L. S. The multi-configurational time-dependent Hartree approach. *Chem. Phys. Lett.* **1990**, *165*, 73–78.

(77) Trenins, G.; Althorpe, S. C. Mean-field Matsubara dynamics: Analysis of path-integral curvature effects in rovibrational spectra. *J. Chem. Phys.* **2018**, *149*, 014102.

(78) Althorpe, S. C. Path-integral approximations to quantum dynamics. *Eur. Phys. J. B* **2021**, *94*, 155.

(79) Ceotto, M.; Atahan, S.; Tantardini, G. F.; Aspuru-Guzik, A. Multiple coherent states for first-principles semiclassical initial value representation molecular dynamics. *J. Chem. Phys.* **2009**, *130*, 234113.

(80) Ceotto, M.; Atahan, S.; Shim, S.; Tantardini, G. F.; Aspuru-Guzik, A. First-principles semiclassical initial value representation molecular dynamics. *Phys. Chem. Chem. Phys.* **2009**, *11*, 3861–3867.

(81) Miller, W. H. Classical S Matrix: Numerical Application to Inelastic Collisions. *J. Chem. Phys.* **2003**, *53*, 3578–3587.

(82) De Leon, N.; Heller, E. J. Semiclassical quantization and extraction of eigenfunctions using arbitrary trajectories. *J. Chem. Phys.* **1983**, *78*, 4005–4017.

(83) Heller, E. J. Frozen Gaussians: A very simple semiclassical approximation. *J. Chem. Phys.* **1981**, *75*, 2923–2931.

(84) Herman, M. F.; Kluk, E. A semiclasical justification for the use of non-spreading wavepackets in dynamics calculations. *Chem. Phys.* **1984**, *91*, 27–34.

(85) Kay, K. G. Integral expressions for the semiclassical time dependent propagator. *J. Chem. Phys.* **1994**, *100*, 4377–4392.

(86) Kay, K. G. Semiclassical propagation for multidimensional systems by an initial value method. *J. Chem. Phys.* **1994**, *101*, 2250–2260.

(87) Kay, K. G. Numerical study of semiclassical initial value methods for dynamics. *J. Chem. Phys.* **1994**, *100*, 4432–4445.

(88) Sepúlveda, M. A.; Grossmann, F. Time-Dependent Semiclassical Mechanics. *Adv. Chem. Phys.* **1996**, *96*, 191–304.

(89) Grossmann, F.; Xavier Jr, A. L. From the coherent state path integral to a semiclassical initial value representation of the quantum mechanical propagator. *Phys. Lett. A* **1998**, *243*, 243–248.

(90) Grossmann, F. A semiclassical hybrid approach to many particle quantum dynamics. *The Journal of Chemical Physics* **2006**, *125*, 014111.

(91) Begusic, T.; Tapavicza, E.; Vanicek, J. Applicability of the thawed Gaussian wavepacket dynamics to the calculation of vibronic spectra of molecules with double-well potential energy surfaces. *J. Chem. Theory Comput.* **2022**, *18*, 3065–3074.

(92) Malpathak, S.; Church, M. S.; Ananth, N. A semiclassical framework for mixed quantum classical dynamics. *J. Phys. Chem. A* **2022**, *126*, 6359–6375.

(93) Malpathak, S.; Ananth, N. Non-linear correlation functions and zero-point energy flow in mixed quantum classical semiclassical dynamics. *The Journal of Chemical Physics* **2023**, *158*, 104106.

(94) Church, M. S.; Ananth, N. Semiclassical dynamics in the mixed quantum classical limit. *The Journal of Chemical Physics* **2019**, *151*, 134109.

(95) Bonnet, L. Semiclassical initial value theory of rotationally inelastic scattering: Some remarks on the phase index in the interaction picture. *The Journal of Chemical Physics* **2018**, *148*, 194104.

(96) Bonnet, L. Semiclassical initial value representation: From Møller to Miller. *The Journal of Chemical Physics* **2020**, *153*, 174102.

(97) Bonnet, L. Semiclassical initial value representation: From Møller to Miller. II. *The Journal of Chemical Physics* **2023**, *158*, 114112.

(98) Conte, R.; Parma, L.; Aieta, C.; Rognoni, A.; Ceotto, M. Improved semiclassical dynamics through adiabatic switching trajectory sampling. *The Journal of Chemical Physics* **2019**, *151*, 214107.

(99) Ceotto, M.; Di Liberto, G.; Conte, R. Semiclassical Divide and Conquer method for spectroscopic calculations of high dimensional molecular systems. *Phys. Rev. Lett.* **2017**, *119*, 010401.

(100) Di Liberto, G.; Conte, R.; Ceotto, M. Divide and conquer semiclassical molecular dynamics: A practical method for spectroscopic calculations of high dimensional molecular systems. *J. Chem. Phys.* **2018**, *148*.

(101) Gabas, F.; Di Liberto, G.; Ceotto, M. Vibrational investigation of nucleobases by means of divide and conquer semiclassical dynamics. *J. Chem. Phys.* **2019**, *150*.

(102) Cazzaniga, M.; Micciarelli, M.; Gabas, F.; Finocchi, F.; Ceotto, M. Quantum Anharmonic Calculations of Vibrational Spectra for Water Adsorbed on Titania Anatase (101) Surface: Dissociative versus Molecular Adsorption. *J. Phys. Chem. C* **2022**, *126*, 12060–12073.

(103) Gabas, F.; Conte, R.; Ceotto, M. Quantum vibrational spectroscopy of explicitly solvated thymidine in semiclassical approximation. *J. Phys. Chem. Lett.* **2022**, *13*, 1350–1355.

(104) Gandolfi, M.; Rognoni, A.; Aieta, C.; Conte, R.; Ceotto, M. Machine learning for vibrational spectroscopy via divide-and-conquer semiclassical initial value represen-

tation molecular dynamics with application to N-methylacetamide. *J. Chem. Phys.* **2020**, *153*.

(105) Moscato, D.; Gabas, F.; Conte, R.; Ceotto, M. Vibrational spectroscopy simulation of solvation effects on a G-quadruplex. *J. Biomol. Struct. Dyn.* **2023**, 1–11.

(106) Zhang, S. L.; Michaelian, K. H.; Loppnow, G. R. Vibrational spectra and experimental assignments of thymine and nine of its isotopomers. *The Journal of Physical Chemistry A* **1998**, *102*, 461–470.

(107) Jorgensen, W. L. Quantum and statistical mechanical studies of liquids. 10. Transferable intermolecular potential functions for water, alcohols, and ethers. Application to liquid water. *J. Am. Chem. Soc.* **1981**, *103*, 335–340.

(108) Urey, H. C.; Bradley Jr, C. A. The vibrations of pentatonic tetrahedral molecules. *Phys. Rev.* **1931**, *38*, 1969.

(109) Miertus, S.; Scrocco, E.; Tomasi, J. Electrostatic interaction of a solute with a continuum. A direct utilizaion of AB initio molecular potentials for the prevision of solvent effects. *Chem. Phys.* **1981**, *55*, 117–129.

(110) Cammi, R.; Tomasi, J. Remarks on the use of the apparent surface charges (ASC) methods in solvation problems: Iterative versus matrix-inversion procedures and the renormalization of the apparent charges. *J. Comput. Chem.* **1995**, *16*, 1449–1458.

(111) Cances, E.; Mennucci, B.; Tomasi, J. A new integral equation formalism for the polarizable continuum model: Theoretical background and applications to isotropic and anisotropic dielectrics. *J. Chem. Phys.* **1997**, *107*, 3032–3041.

(112) Barone, V.; Cossi, M. Quantum calculation of molecular energies and energy gradients in solution by a conductor solvent model. *J. Phys. Chem. A* **1998**, *102*, 1995–2001.

(113) Scalmani, G.; Frisch, M. J. Continuous surface charge polarizable continuum models of solvation. I. General formalism. *J. Chem. Phys.* **2010**, *132*, 114110.

(114) Mennucci, B. Polarizable continuum model. *Wiley Interdisciplinary Reviews: Computational Molecular Science* **2012**, *2*, 386–404.

(115) Jeziorski, B.; Moszynski, R.; Szalewicz, K. Perturbation theory approach to intermolecular potential energy surfaces of van der Waals complexes. *Chemical Reviews* **1994**, *94*, 1887–1930.

(116) Werner, H.-J.; Knowles, P. J.; Manby, F. R.; Black, J. A.; Doll, K.; Heelmann, A.; Kats, D.; Kohn, A.; Korona, T.; Kreplin, D. A., et al. The Molpro quantum chemistry package. *The Journal of chemical physics* **2020**, *152*.

(117) Colbert, D. T.; Miller, W. H. A novel discrete variable representation for quantum mechanical reactive scattering via the Smatrix Kohn method. *The Journal of chemical physics* **1992**, *96*, 1982–1991.

(118) Belyaev, A. K.; Colbert, D. T.; Groenenboom, G. C.; Miller, W. H. State-to-state reaction probabilities for $H - +H2, D2$ collisions. *Chemical physics letters* **1993**, *209*, 309–314.

Graphical TOC Entry